Charging a electrical double layer supercapacitor exhibiting a distribution of relaxation times

*L.E. Helseth**

Department of Physics and Technology, Allegaten 55, 5020 Bergen, University of Bergen, Norway

*Corresponding author

Email: Lars.Helseth@uib.no

ABSTRACT: A charging regular electrical double layer supercapacitor can usually be described by a single capacitance and a single resistance in parallel, wherein the latter represents the ohmic losses. Such ideal behavior may occur if the supercapacitor consists of self-similar porous carbon micro- and nanostructures. However, if the regular supercapacitor consists of a sequence of slices with different relaxation times, a strong deviation from ideal charging curves may occur. Here, it is demonstrated how such charging curves can be interpreted in terms of a distribution of relaxation times. It is found that in presence of a broad distribution of charge transfer resistances, the voltage initially appears to increase faster than normal during galvanostatic charging. Care should be taken to avoid misinterpretation of the capacitance under such circumstances.

KEYWORDS: Supercapacitor, charging, distribution of relaxation times

1. Introduction

Supercapacitors are electrochemical double layer capacitors utilizing an electrolyte in contact with a porous carbon surface [1-4]. The electrolyte contains a large concentration of ions which form an electrical double layer on a micro and nanostructured carbon surface [4-6]. The performance and degradation of supercapacitors is often measured using impedance spectroscopy, cyclic voltammetry or galvanostatic charging, and modelling of these processes undertaken using equivalent electric circuits [7-11]. Of particular interest is the capacitance of a supercapacitor, which is related to its ability to store electrical charge.

Upon charging, the amount of charge associated with the carbon surface increases gradually, and the current I through the supercapacitor is assumed to be I=CdV/dt, where dV/dt is the voltage change rate and C the capacitance [12,13]. This definition does not account for any resistive processes taking place during charging, and recent works have demonstrated that care must be taken when interpreting the found capacitance [14,15]. In fact, it has recently been demonstrated that the nonlinearities in galvanostatic charging curves of a range of commercial supercapacitors are well modelled using a simple Randles-like resistance-capacitance parallel circuit, and that such a circuit can explain how the charging depends on applied current and temperature [16]. However, in the literature strongly nonlinear charging curves that cannot be modelled using such a simple circuit are sometimes reported for newly developed supercapacitors, in particular metal-free variants which lack a highly conducting metal substrate [17-19]. In the current work it is demonstrated that these charging curves can be interpreted in terms of a distribution of relaxation times associated with a distribution of charge transfer resistances.

2. Background

A regular supercapacitor consists of self-similar hierarchical micro and nanostructures, which in ref. [16] was shown to be associated with a resistance-capacitance parallel circuit associated with a fixed relaxation

time. The reason for this is that only a limited set of pore-sizes are accessed for a given current. Large charging currents only allow one to access the largest pores. The smaller ones are clogged by ions trying to penetrate into them, and do not become unclogged unless one waits for a long time or change the current. If one wants to access the smallest pores, one needs to apply a small current. This takes longer time, but avoids aggregation and clogging. As demonstrated in ref. [16], the relaxation time is inversely proportional to the current. A natural consequence of the observations described above and in previous publications [15-16] is that a regular supercapacitor can be well described by a single parallel RC-circuit, i.e. a resistor R_1 and a capacitor C_1 in parallel, in series with a resistor R_{s1}. This corresponds to the leftmost unit in fig. 1.

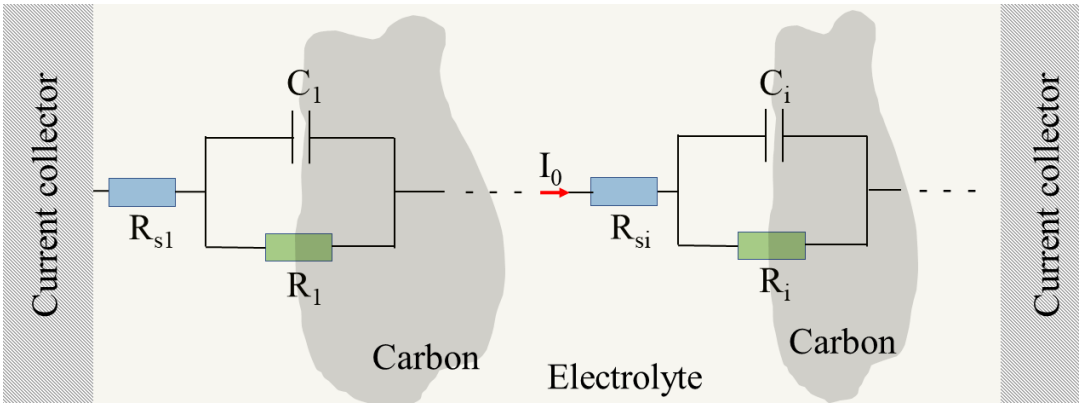

Figure 1. Schematic drawing of the system under consideration, showing two pieces of microstructured carbon surrounded by electrolyte. Here I_0 is the constant current passing through each localized slice of capacitance C_i and charge transfer resistance R_i. The local bulk contribution to the resistance, due to either contact or electrolyte, is denoted R_{si}.

A single RC-circuit (the leftmost R_1C_1-circuit in fig.1) was analyzed in detail in refs. [15-16] and is not the main topic of the current work. The goal of the current work is to show that certain supercapacitors may have a layered structure consisting of several serial layers of RC-circuits, thus resulting in a

distribution of relaxation times. Fig. 1 shows a schematic drawing of the structure and buildup of such a layered supercapacitor. The porous structure in the supercapacitor can be divided into thin, stacked slices, each of which must pass the entire constant current I_0 during charging. Consider a localized thin slice of area A_i on the porous carbon surface of a supercapacitor. When a current is applied, charge is gradually built up and stored on the surface area A_i of the porous carbon with a surface charge density σ_i, such that the charge is given by $q_{si}=\sigma_i A_i$. Another amount of charge q_{ri} is lost due to charge transfer from faradaic reactions. The total charge transferred to the is $q_i=q_{ri}+q_{si}$, giving rise to a current given by

$$I_0 = I_{si} + I_{ri} = A_i \frac{d\sigma_i}{dt} + \frac{dq_{ri}}{dt} \quad . \tag{1}$$

The charge and voltage are often related in a nearly linear fashion on a global scale [20]. It is reasonable to assume that such a linear relationship also holds locally, and therefore to define a local constant capacitance C_i which relates the surface charge and the corresponding voltage V_i according to

$$\sigma_i = \frac{C_i}{A_i} V_i \quad . \tag{2}$$

The charge loss q_{ri} can occur in different forms, but here we will exemplify it due to a charge transfer caused by faradaic reactions alone. That is, it is assumed that the electrolyte concentration is large enough and the grain structure properly wetted, such that electrolyte starvation caused by diffusion is negligible [21]. The charge transfer due to faradaic reactions may in the simplest approximation be given by the Butler-Volmer equation [22]

$$I_{ri} = I_{riA}\left(e^{\alpha eV_i/k_BT} - e^{-(1-\alpha)eV_i/k_BT}\right) \quad , \tag{3}$$

where α is the transfer coefficient, $e=1.6\cdot10^{-19}$ C is the electric charge, $k_B=1.38\cdot10^{-23}$ J/K, T is the temperature and I_{riA} is the exchange current density which depends on the surface concentration of the redox-species as well as the rate at which they are transformed. For small voltages ($eV/k_BT \ll 1$) one may write

$$I_{ri} \approx \frac{V_i}{R_i} \quad , \quad R_i = \frac{k_BT}{eI_{riA}} \quad , \tag{4}$$

such that R_i is the charge transfer resistance. Under most circumstances one does not have small voltages, but we will nonetheless make the assumption that the losses can be accounted for by a ohmic resistance R_i which gives a linear relationship between applied current and voltage over the charging pores.

According to eqs. (1), (2) and (4), the total current can be written as

$$I_0 = C_i \frac{dV_i}{dt} + \frac{V_i}{R_i} \quad . \tag{5}$$

Let us now consider the situation where the carbon surface is initially uncharged, such that $V_i(t=0)=0$, and that the current I_0 is constant. After a certain time, the localized voltage is

$$V_i(t) = I_0R_i\left(1 - e^{-t/\tau_i}\right) \quad , \quad \tau_i = R_iC_i \quad . \tag{6}$$

The supercapacitor consists of a sequence of slices in series, and the total voltage over the entire supercapacitor is therefore a sum over all the local voltages, where each contribution is weighted with a factor P_i such that $I_0R_i=I_0R_pP_i$. Here R_p represents the singular value of the charge transfer resistance

which occurs when there is only one relaxation time present during charging such that P_i=1 and R_i =R_p. Note that P_i describes the distribution of resistances through the elongated porous structure. P_i can be entirely ascribed to the charge transfer resistance. We will proceed under the assumption that it is there is a distribution of charge transfer resistances and therefore also relaxation times τ_i=R_iC_i. The total voltage is a sum over all local slices and given by

$$V_C(t) = \sum_{i=1}^{N} V_i(t) + \sum_{i=1}^{N} R_{si} I_0 = I_0 R_p \sum_{i=1}^{N} P_i\left(1 - e^{-t/\tau_i}\right) + R_s I_0 \quad . \qquad (7)$$

As in refs. [14-16], the voltage drop due to a series resistance $R_s = \sum_{i=1}^{N} R_{si}$ is added to allow for ohmic resistance due to the bulk electrolyte or contact between carbon and metal current collector. Equation (7) can be understood by noting that each individual region of the porous carbon surface may have a charge transfer resistance R_i which differs from the other regions, and which governs both the probability weight factor P_i and the relaxation time τ_i. On the other hand, the local capacitances C_i only influence the relaxation time. If a supercapacitor is made such that R_i, and therefore also τ_i is large, one may in many cases set $t \ll \tau_i$ for the time interval of interest during charging. Then eq. (7) can be written as

$$V_C(t \ll \tau_i) \approx I_0 t \sum_{i=1}^{N} \frac{1}{C_i} + R_s I_0 \quad . \qquad (8)$$

From eq. (8) it is seen that the voltage increases linearly with time and the total capacitance is that of N capacitances connected electrically in series. This is sometimes considered the ideal behavior of a supercapacitor, and explains why a probability distribution of capacitances similar to P_i for resistances has not so far been needed when describing a regular supercapacitor.

Assume that the many contributed charge transfer resistances have a continuous distribution $P(\tau)$ such that one can replace equation (7) with an integral:

$$V_C(t) = I_0 R_p \int_0^\infty P(\tau)\left(1 - e^{-t/\tau}\right) d\,\tau + R_s I_0 \quad . \tag{9}$$

We introduce a new variable s and a constant τ_0 such that $s=\tau_0/\tau$. Here it is required that the distribution fulfills the condition $\int_0^\infty P(s) d\,\tau = 1$. Equation (8) can now be written as

$$V_C(t) = \left(R_s + R_p\right) I_0 - I_0 R_p \int_0^\infty P(s) e^{-s\left(\frac{t}{\tau_0}\right)} d\,s \quad . \tag{10}$$

To obtain the distribution P(s) from the measured voltage V_C during charging using the integral in eq. (10) is in general rather challenging, in particular since the charge transfer resistances usually are rather large such that the voltage-time curve is nearly linear. However, there are situations where deviations from linearity are significant, and a particular convenient representation of the voltage occurs if one sets

$$\int_0^\infty P(s,\beta) e^{-st/\tau_0} d\,s = e^{-\left(\frac{t}{\tau_0}\right)^\beta}, \tag{11}$$

where τ_0 is a constant that may be used to estimate the order of magnitude of the expected relaxation time, but care should be taken not to give it an interpretation as some sort of general time decay constant [23]. Note that β is also constant which provides useful information about the width of the distribution P(s, β). When β=1, the distribution P(s,β) is a Dirac delta function centered on τ_0. Only when β=1, the constant τ_0 truly represents the actual decay rate. When the parameter β decreases, the distribution of relaxation times broadens and indicates that one has a layered distribution of pore sizes or interfacial voids. P(s,β) has been tabulated numerically for a range of values of β in ref. [24]. It is also known analytically for particular values of β such as β=1/2, as detailed in ref. [23]. By setting $x=t/\tau_0$ in eq. (11), the Laplace transform is given by [23,24]

$$P(s,\beta) = \frac{1}{2\pi i}\int_{-i\infty}^{+i\infty} e^{-(x)^{\beta}} e^{sx} dx \quad . \tag{12}$$

Analytical solutions of eq. (13) are found only in a few cases like β=0.5, and it is therefore most convenient to use numerical tables when extracting the distribution or arbitrary values of the coefficient in the range 0<β<1 [24].

Using eq. (11), the voltage over the supercapacitor becomes

$$V_C(t) = R_s I_0 + I_0 R_p \left[1 - e^{-\left(\frac{t}{\tau_0}\right)^{\beta}}\right] \quad . \tag{12}$$

The charging curve depends on the parameter β. Since for a given current I_0 it is likely that only a fixed set of pores are accessed, it is expected that β remains constant during charging.

Fig. 2 a) shows three examples of voltage versus time charging curves using eq. (12). The solid black line corresponds to β=1, the red dash-dotted curve to β=0.9 and the blue dashed curve to β=0.4. The difference between β=1 and β=0.9 is very small, and is unlikely to be easy to detect from experimental data. The distribution P(s) for β=1 is a sharp line at s=1, whereas the corresponding distribution for β=0.9 is displayed as a red dash-dotted curve in fig. 2 b). For values of beta significantly different from one, the voltage-time curve shows highly nonlinear behavior. For example, the case β=4 is shown as a blued dashed line in fig. 2 a), and the corresponding distribution P(s,β) is displayed in fig. 2 b). it is noted that the voltage initially increases much faster than for β=1, but then flatten gradually out. This is due to the large distribution of relaxation times displayed by the blue dashed line in fig. 2 b). The smaller relaxation times allow a fast initial response. However, soon they are fully charged and any additional response must be due to the longer relaxation times. In general, one observes that for β<1 the voltage increases faster

with time than when $\beta=1$ as long as $t<\tau_0$, where 63% of the maximum voltage has been reached. However, when $t>\tau_0$ the increase in voltage is slower for $\beta<1$ than for $\beta=1$. From this one can conclude that fast modes with small relaxation times are quickly charged for $\beta<1$, whereas for $\beta=1$ there is only one relaxation mode which determines the charging time. However, one should also be aware that these are lossy modes, since the charge transfer resistance represent loss mechanisms in the model considered here.

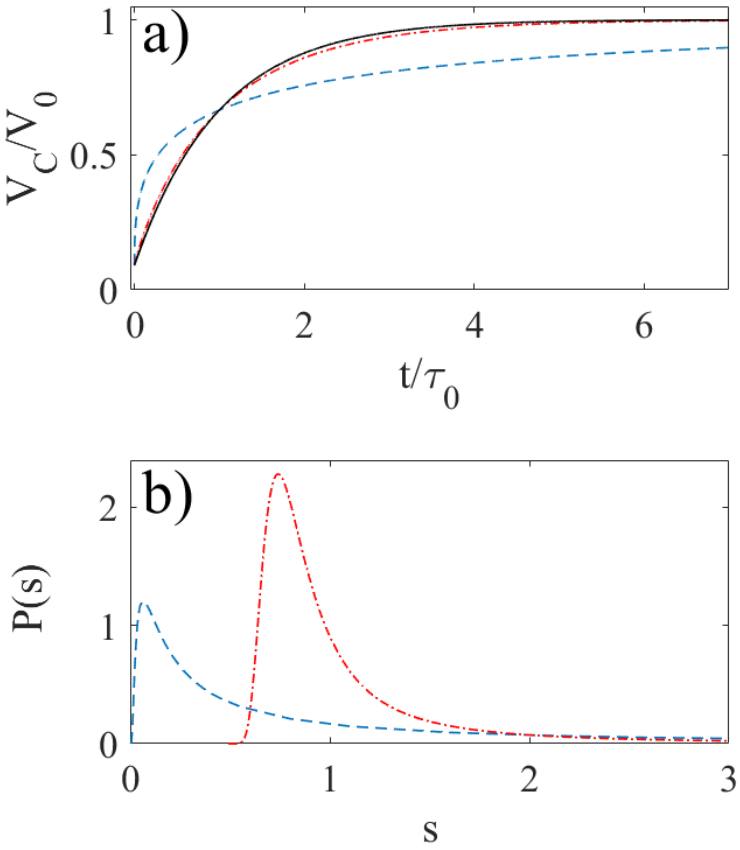

Figure 2. The voltage over a supercapacitor versus the reduced time t/τ_0 for $\beta=1$ (black curve), $\beta=0.9$ (red dash-dotted curve) and $\beta=0.4$ (blue dashed curve). In b), the distributions for $\beta=0.9$ (red dash-dotted curve) and $\beta=0.4$ (blue dashed curve) are shown.

3. Discussion

In the literature, nonlinear charging curves have often been interpreted in terms of a voltage-dependent capacitance [25], which has been explained in terms of the perfectly smooth theory of electrical double layers [26] or due to voltage-dependent dipole orientation [27]. However, supercapacitors composed of micro and nanostructured carbon immersed in electrolyte do not have flat active surfaces, but are made of irregular surfaces supporting both dissipative and charge storage processes. In ref. [16] it was demonstrated that all supercapacitors exhibiting a single relaxation time (i.e. N=1 in eq. (7)) can be well described by a single equivalent circuit for different capacitances, currents and temperatures. That is, the analysis of ref. [16] is only valid when each of the slices of fig. 1 can be described by the same relaxation time (i.e. the same parallel resistance and capacitance). This is the case for well-mixed porous carbon surfaces wherein a self-similar porous carbon structure occurs throughout the volume of the supercapacitor. However, under some circumstances one may expect that the porous carbon structure is sequentially distributed, which means that in some slice-regions the relaxation time is large while in others it is small, such that several different relaxation times occur. In this case, one should refer to eq. (9) as described in the current work. The parameter β in eq. (12) can be used as a first approach to determine how a layered structure may influence the charging performance of a supercapacitor, and thereby allowing one to access the layered distribution of pore sizes or interfacial voids through the distribution of relaxation times. However, if one wants to know correlations between β and the geometrical structure, precise experiments wherein the layered structure is mapped by for example electron microscopy, followed by corresponding charging curves, must be investigated. Such correlated data are not available in the literature, and therefore must await future experiments.

Nonetheless, the theory presented in the previous section can be used to interpret existing data reported in the literature. An example to which the theory most likely can be applied is reported in ref. [17], were several different samples with various weight ratios of nanographite to activated carbon were used to form metal-free supercapacitors. Sample A was made with 50 wt% nanographite and 50 wt% activated carbon,

sample B with 40 wt% nanographite and 60 wt% activated carbon, sample C with 30 wt% nanographite and 70 wt% activated carbon, and sample D with 20 wt% nanographite and 80 wt% activated carbon. The voltage during charging of the resulting supercapacitors was reported in ref. [17], and the data was extracted from the figures of that work using a MatLab script called grabit.m.

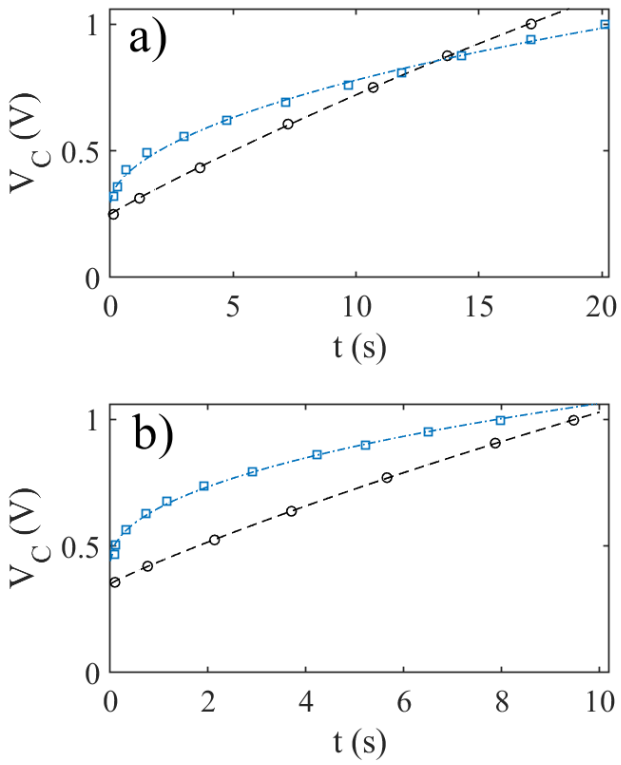

Figure 3. The charging voltage over the metal-free supercapacitors reported in fig. 4 in ref. [17] made with 50 wt% nanographite and 50 wt% activated carbon (black circles) and 20 wt% nanographite and 80 wt% activated carbon (blue squares). The charging currents were 1.6 A/g (a) and 2.4 A/g (b).

The black circles in fig 2 a) shows the voltage during charging for sample A during charging with a current 1.6 A/g presented in fig. 4 e) in ref. [17]. The black, dashed line is a fit to eq. (12) with $V_s = R_sI_0 = 0.25$ V, $R_pI_0 = 3.5$V, $\tau_0 = 75$ s and β=0.97. The coefficient of determination is R^2=0.9997, which indicates a good fit. It is found that fixing β=1 and $R_pI_0 = 3.5$V gives a fit with $\tau_0 = 70$ s at R^2=0.9993, but that the fit

could be improved to R^2=0.9998 by letting also R_p vary freely. Since the voltage-time curve is nearly linear, the capacitance is fixed by $C_1=I_0/dV_C/dt$, which is (31±1) C/g in this particular case. While the fits like the black dashed line in fig. 2 a) are nearly linear and therefore allow a well-defined capacitance, the parallel resistance may take on much larger variations with just minor adjustments of the fitting curve. For example, a fitting curve like the black dashed curve in fig. 2a) gives rise to R_p=2.2 Ωg with R^2=0.9993, while a fit with the same capacitance, R_p=1.5 Ωg gives R^2=0.9998. From this one can conclude that nearly linear curves can only extract parallel resistance R_p with rather large uncertainty, and that eq. (11) is of no particular value in this case.

However, a completely new situation emerges if the curves are highly nonlinear. The blue squares in fig. 2 a) shows the voltage of sample D in ref. [17] during charging with a current 1.6 A/g, and the dash-dotted blue line is a fit of eq. (12) with $V_s=R_sI_0$ = 0.30 V, R_pI_0 = 3.5 V, τ_0 = 303 s, β = 0.56 and R^2=0.9963. Attempting to fix β=1 gives at best R^2=0.9727, which is a notably poorer fit. Thus, the strong increase, followed by a flattening in voltage of as seen by the blue squares in fig. 2 a) therefore represent a strongly nonlinear behavior that is better represented by a distribution rather than a single relaxation time. Similar considerations can also be given the other curves. By fitting eq. (12) to charging voltages for samples A, B, C and D, it is found that β becomes 0.96 (sample A), 0.92 (sample B), 0.73 (sample C) and 0.56 (sample D). These findings indicate that the distribution of charge transfer resistances gradually increase as one creates samples with gradually higher content of activated carbon.

While the nonlinear eq. (12) does indeed represent the experimental data well, it is worth pointing out that reversible charge transfer processes galvanostatic charging curve may exhibit a steep initial curvature followed by a flatter region in a similar manner as that observed for samples D in fig. 4 e) of ref. [17]. Entirely reversible charge transfer reactions, such as seen in rechargeable batteries, are sometimes explained by considering the time-dependent ion concentration obtained using diffusion equation in

combination with the Nernst equation to obtain the time-dependent voltage as $V_C=V_1+(RT/nF)\ln[(\tau_A^{1/2}-t^{1/2})/t^{1/2}]$. Here R is the universal gas constant, F is the Faraday constant, V_1 is a constant, n is the number of moles of electrons participating in the charge transfer reaction, and τ_A is a characteristic time which can be estimated using the Sand equation [28]. This equation for the voltage is sometimes used to explain the charging of rechargeable batteries. It is seen that the voltage eventually starts to increase significantly as $t\rightarrow\tau_A$. However, there is no indication of such reversible charge transfer reactions occur in supercapacitors such as that manufactured in ref. [17]. Under such conditions it is reasonable to apply eq. (12).

Similar behavior as seen in fig. 2 a) is found also for other charging currents for samples reported in ref. [17]. The black circles in fig. 2 b) shows the voltage during charging for sample A during charging with a current 2.4 A/g as shown in fig. 4 f) in ref. [17]. The black, dashed line is a fit to eq. (12) with $V_s=R_sI_0=0.35$ V, $R_pI_0=3.5$V, $\tau_0=52$ s, $\beta=0.93$ with $R^2=0.9999$. Also here a fit to a curve with a single relaxation time (i.e. $\beta=1$) is possible with a high coefficient of determination $R^2=0.9999$. One can therefore not interpret a fit with $\beta=0.93$ as due to a distribution of relaxation time constants since a fit with a single time constant would do equally well at least when using the R^2 – value or by a visual inspection. This is not so for sample D in fig. 4 f) in ref. [17]. The blue squares in fig. 2 b) show the voltage of sample D during charging with current 2.4 A/g, and the dash-dotted blue line is a fit of eq. (12) with $V_s=R_sI_0=0.44$ V, $R_pI_0=3.5$ V, $\tau_0=262$ s, $\beta=0.50$ with $R^2=0.9944$. Attempting to fix $\beta=1$ gives at best $R^2=0.9678$, which is a poorer fit that does not represent the experimental data as well as eq. (12) with $\beta=0.50$. A curve with $\beta=0.50$ can be understood as a due to a broad tail of relaxation coefficients caused by a broad range of charge transfer resistances. The origin of the distribution of charge transfer resistances could be related to the relatively larger interfaces generated by micron sized activated carbon which in ref. [17] was reported to reduce adhesion and increase deformation during drying. This again might be related to change in size and shape during drying, which could cause a large number of different

interactions with the nanographite flakes. In ref. [17] it was hypothesized that comparably large cavities and poor contacts were the reason for the nonlinear charging curves. Here we hypothesize that this is consistent with the interpretation of the results in terms of a distribution of charge transfer resistances in sample D during charging. While strong adhesion may result in larger contact regions with larger contact area and therefore smaller charge transfer resistance, smaller regions may give rise to larger charge transfer resistance.

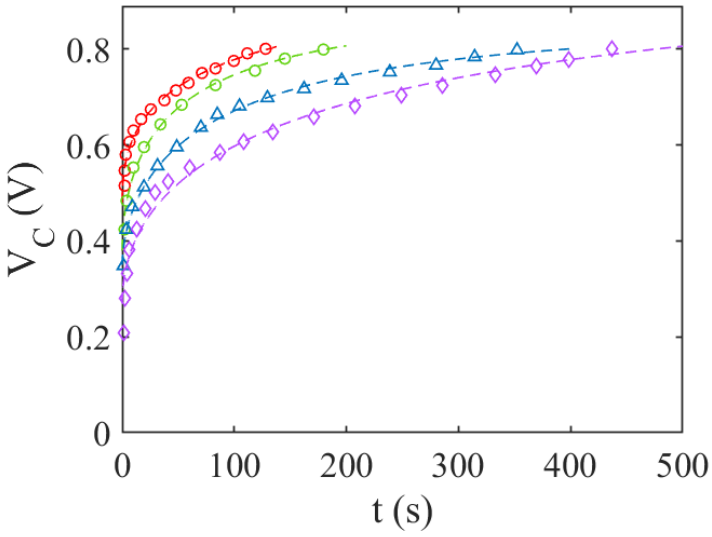

Figure 4. The red circles (slurry 1), green boxes (slurry 2), the blue triangles (slurry 3) and violet diamonds (slurry 4) are data points grabbed from ref. [18] using grabit.m. The dashed lines are fits to the experimental data using eq. (12).

Another system in which a distribution of relaxation times may play a role is the case of 3D-printed metal free supercapacitors as those presented in ref. [18]. In ref. [18] slurries of carbon conductive paint and water at different concentrations were used to print supercapacitors, with a hydrogel composed of polyvinyl alcohol and phosphoric acid acting as a gel electrolyte. Data points were extracted from ref.

[18] using grabit.m, and shown in fig. 4 for concentrations 4.8 % (slurry 1, red circles), 7.0 % (slurry 2, green circles), 9.1 % (slurry 3, blue triangles) and 11.1% (slurry 4, violet diamonds).

The red dashed line is a fit to eq. (12) with $V_s = R_sI_0 = 0.50$ V, $R_pI_0 = 0.5$V, $\tau_0 = 123$ s and $\beta=0.46$, $R^2=0.9803$. The green dashed line is a fit to eq. (12) with $V_s = R_sI_0 = 0.38$ V, $R_pI_0 = 0.5$V, $\tau_0 = 60$ s and $\beta=0.55$, $R^2=0.9909$. The blue dashed line is a fit to eq. (12) with $V_s = R_sI_0 = 0.35$ V, $R_pI_0 = 0.5$V, $\tau_0 = 95$ s and $\beta=0.59$, $R^2=0.9930$. Finally, the violet dashed line is a fit to eq. (12) with $V_s = R_sI_0 = 0.27$ V, $R_pI_0 = 0.7$V, $\tau_0 = 243$ s and $\beta=0.52$, $R^2=0.9715$. It should be emphasized that fits to eq. (12) assuming $\beta=1$ gave poor fits and are therefore not reported here.

As reported in ref. [18], the number of deposits needed to make the required thickness (0.5 mm) decreased with the concentration of conductive carbon, from 5 deposits at 4.8 % concentration to only 2 deposits at 11.1 % concentration. This may explain the fact that β appears to be increasing with the slurry concentration, with $\beta=0.46$ at 4.8%, $\beta=0.55$ at 7.0% and $\beta=0.59$ at 9.1 %. A small decrease to $\beta=0.52$ is then seen at 11.1 %, but the overall impression is an increase in β with concentration. This increase in β suggests that there should be a broader distribution of relaxation times as well. One may then argue that when the concentration of carbon particles increases, fewer 3D-printed layers are needed, which may result in fewer layer-transitions. One may imagine that near such a transition between layers, the particles are arranged differently than in the bulk of a layer, thus giving rise to a different relaxation time. At the same time, the interfacial series resistance R_s increases with number of layers as indicated in fig. 4. Therefore, having more layers means creating more opportunity for carbon particles to arrange in different manners with different relaxation times. While these arguments are appealing, further designated experiments correlating micro and nanostructure with galvanostatic charging curves are needed in order to verify their validity. However, such work is outside the scope of the current study.

4. Conclusion

In this work galvanostatic charging of a supercapacitor which exhibits a distribution of relaxation times is examined. It is found that a broad distribution of relaxation times gives rise to a faster increase in voltage than a narrow distribution. It is shown how a distribution of charge transfer resistances can be used to explain experimental data found in the literature for metal-free supercapacitors. The work presented here accounts for charge storage on the porous surface combined with resistive loss mechanisms. Under some circumstances, for instance in pseudocapacitors, one would be interested also in faradaic charge transfer facilitated by redox-reactions. One could account for such mechanisms through additional terms added to eq. (5), but this is outside the scope of the current work.

REFERENCES

(1) H. I. Becker, U.S. pat., 2800.616 to General Electric Co. (1957).

(2) B. E. Conway, Electrochemical Supercapacitors, Kluwer Academic, New York, USA (1999).

(3) J.R. Miller, "Engineering electrochemical capacitor applications", J. Power Sources, **326**, 726-735, (2016).

(4) B.B. Garcia, A.M. Feaver, Q. Zhang, R.D. Champion, G. Zhao, T.T. Fister, K.P. Nagle and G.T. Seidler, "Effect of pore morphology on the electrochemical properties of electric double layer carbon cryogel supercapacitors", J. Appl. Phys, **104**, 014305 (2008).

(5) L.M. Da Silva, R. Cesar, C.M.R. Moreira, J.H.M. Santos, L.G. De Souza, B.M. Pires, R. Vincentini, W. Nunes and H. Zanin, "Reviewing the fundamentals of supercapacitors and the difficulties involving the analysis of the electrochemical findings obtained for porous electrode materials", Energy Storage Materials, **27**, 555-590 (2020).

(6) S. Satpathy, S. Das, B.K. Bhattacharyya, "How and when to use super-capacitors effectively, an integration of review of past and new characterization works on super-capacitors", J. Energy Storage **27**, 101044 (2020).

(7) D.P. Dubal, Y.P. Wu and R. Holze, "Supercapacitors: from the Leyden jar to electric buses", ChemTexts, **2**, 13 (2016).

(8) I.N. Jiya, N. Gurusinghe and R. Gouws, "Electrical circuit modelling of double layer capacitors for power electronics and energy storage applications: A review", Electronics, **7**, 268 (2018).

(9) Poonam, K. Pareek and D.K. Jangid, "Analysis of the effect of different factors on the degradation of supercapacitors", Ionics, https://doi.org/10.1007/s11581-022-04650-z (2022).

(10) Poonam, M. Vyas, D.K. Jangid, R. Rohan and K. Pareek, "Investigation of supercapacitor degradation through impedance spectroscopy and Randles circuit model", Energy Storage, e355, 1-6 (2022), DOI: 10.1002/est2.355.

(11) R.T. Yadlapalli, R.R. Alla, R. Kandipati and A. Kotapati, "Super capacitors for energy storage: Progress, applications and challenges", J. Energy Storage, 49, 104194 (2022).

(12) C. Lämmel, M. Schneider, M. Weiser and A. Michaelis, "Investigations of electrochemical double layer capacitor (EDLC) materials - a comparison of test methods", Mat.-wiss. U. Werkstofftech., **44**, 641-649 (2013).

(13) Y. Ge, X. Xie, J. Roscher, R. Holze and Q. Qu, "How to measure and report the capacity of electrochemical double layers, supercapacitors, and their electrode materials", J. Solid State Electrochemistry, **24**, 3215-3230 (2020).

(14) L.E. Helseth, "Modelling supercapacitors using a dynamic equivalent circuit with a distribution of relaxation times", J. Energy Storage, **25**, 100912 (2019**)**.

(15) L.E. Helseth, "Comparison of methods for finding the capacitance of a supercapacitor", J. Energy Storage, **35**, 102304 (2021**)**.

(16) L.E. Helseth, "The nonlinearities in the galvanostatic charging curves of supercapacitors provide insight into charging mechanisms", J. Energy Storage, **55**, 10540 (2022**)**.

(17) N. Blomquist, T. Wells, B. Andres, J. Bäckström, S. Forsberg and H. Olin, "Metal-free supercapacitor with aqueous electrolyte and low-cost carbon materials", Sci. Rep., **7**, 39836 (2017**)**.

(18) A. Tanwilaisiri, Y. Xu, D, Harrison, J. Fyson and M. Arier, "A study of metal free supercapacitors using 3D printing", Internation Journal of Precision Engineering and Manufacturing, **19**, 1071-1079 (2018**)**.

(19) N. Blomquist, R. Koppolu, C. Dahlström, M. Toivakka and H. Olin, "Influence of substrate in roll-to-roll coated nanographite electrodes for metal-free supercapacitors", Sci. Rep., **10**, 5282 (2020**)**.

(20) J.M. Griffin, A.C. Forse, W.Y. Tsai, P.L. Taberna, P. Simon and C.P. Grey, "In situ NMR and electrochemical quartz crystal microbalance techniques reveal the structure of the electrical double layer in supercapacitors", Nature Materials, **14**, 812-819, (2015).

(21) W.G. Pell, B.E. Conway and N. Marincic, "Analysis of non-uniform charge/discharge and rate effects in porous carbon capacitors containing sub-optimal electrolyte concentrations", J. Electroanalytical Chemistry, **491**, 9-21 (2000**)**.

(22) W. Schmickler, "Interfacial Electrochemistry", Oxford University Press (1996).

(23) D.C. Johnston, "Stretched exponential relaxation arising from a continuous sum of exponential decays", Phys. Rev. B, **74**, 184430 (2006**)**.

(24) M. Dishon, J.T. Bendler and G.H. Weiss, "Tables of the inverse Laplace transform of the function $\exp(-s^{\beta})$", Journal of Research of the National Institute of Standards and Technology, **95**, 433-467 (1990).

(25) V. Ruiz, S. Roldan, I. Villar, C. Blanco and R. Santamaria, "Voltage dependence of carbon-based supercapacitors for pseudocapacitance quantification", Electrochimica Acta, **95**, 225-229 (2013**)**.

(26) H. Shao, Y.C. Wu, Z. Li, P.L. Taberna and P. Simon, "Nanoporous carbon for electrochemical capacitive energy storage", Chem. Soc. Rev., **49**, 3005 (2020).

(27) R. He, K.J. Aoki and J. Chen, "Electric field-dependence of double layer capacitances by current-controlled charge-discharge steps", Electrochem, **1**, 217-225 (2020**)**.

(28) R.K. Jain, H.C. Gaur and B.J. Welch, “Chronopotentiometry: A review of theoretical principles”, J. Electroanal. Chem., **79**, 211-236 (1977).